International Journal of Automotive Technology, Vol. 7, No. 1, pp. 109–114 (2006)

1229-9138/2006/025-14

FINITE ELEMENT MODELING AND PARAMETER STUDY OF HALF-BEAD OF MLS CYLINDER HEAD GASKET

S.-S. CHO[1)*], B. K. HAN[1)], J.-H. LEE[1)], H. CHANG[2)] and B. K. KIM[3)]

[1)]Department of Mechanical & System Design Engineering, Hongik University, Seoul 121-791, Korea
[2)]Hyundai Motor Company, 772-1 Jangduk-dong, Hwaseong-si, Gyeonggi 445-706, Korea
[3)]Department of Mechanical & Automotive Engineering, Inje University, Gyeongnam 621-749, Korea

(Received 10 March 2005; Revised 28 July 2005)

ABSTRACT–Half-beads of multi-layer-steel cylinder head gaskets take charge of sealing of lubrication oil and coolant between the cylinder head and the block. Since the head lifts off periodically due to the combustion gas pressure, both the dynamic sealing performance and the fatigue durability are essential for the gasket. A finite element model of the half-bead has been developed and verified with experimental data. The half-bead forming process was included in the model to consider the residual stress effects. The model is employed to assess the dependence of the sealing performance and the fatigue durability on the design parameters of half-bead such as the width and height of bead and the flat region length. The assessment results show that the sealing performance can be enhanced without significant deterioration of the fatigue durability in a certain range of the half-bead width. In the other cases the improvement of sealing performance is accompanied by the loss of the fatigue durability. Among three parameters, the bead width has the strongest influence.

KEY WORDS : MLS(Multi-layer-steel) cylinder head gasket, Half-bead, Sealing, Fatigue, Finite element analysis

1. INTRODUCTION

Multi-layer-steel (MLS) cylinder head gaskets are used for sealing between the head and the block in modern automotive internal combustion engines. The MLS gaskets are made of cold-rolled stainless steel thin plates with elastomer overcoats. The plate is embossed to form two major features, i.e., full-bead and half-bead that are in charge of the sealing of combustion gas and liquid, respectively. The embossed plates that are called the functional layers are stacked to suffice the required sealing performance.

When the gasket is installed between the cylinder head and the engine block by fastening the head bolts, the bead is compressed to be almost flat and generates the contact pressure for the sealing along the line of bead. During the engine operation the combustion gas pressure lifts off the head and thus increases the gap between the head and the block. As the gap is increased, the bead recovers its shape and maintains the contact pressure over the required minimum sealing pressure. In this way the bead carries out its sealing function even when the cylinder head lifts off.

During the periodic gap variation between the head and block the bead is subject to the cyclic compression and recovery, and thus susceptible to the fatigue failure. Hence, the bead is required to possess the sufficient fatigue strength.

Both the sealing performace and the fatigue durability of the gasket must be assured during the development of engines. Conducting the test with the rig as well as the real engine at the design stage is very difficult, expensive and time-consuming (Ishigaki *et al.*, 1993). An alternative approach is to conduct the finite element analysis (Harland *et al.*, 1993; Popielas *et al.*, 2000). The present authors developed a finite element model of the full-bead and demonstrated the reliability of the model in the assessment of sealing performance (Cho *et al.*, 2005) and fatigue durability (Cho *et al.*, 2005).

Although several studies on the full-bead have been published, no study on the half-bead is found in the literature. In this work, a finite element model of the half-bead is introduced and the major design parameters of the half-bead are examined with respect to the sealing perfor-mace and the fatigue durability to provide the guideline for the design of half-bead.

2. FINITE ELEMENT ANALYSIS

Figure 1 shows two stacked half-beads surrounding the lubrication oil or coolant hole between the cylinder head

*Corresponding author. e-mail: sscho@hongik.ac.kr

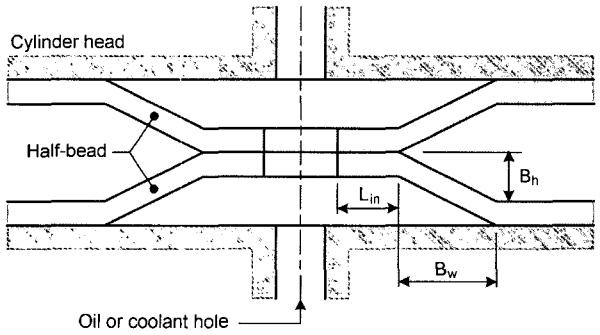

Figure 1. Schematic representation of two stacked half-beads of MLS gasket and the nomenclatures.

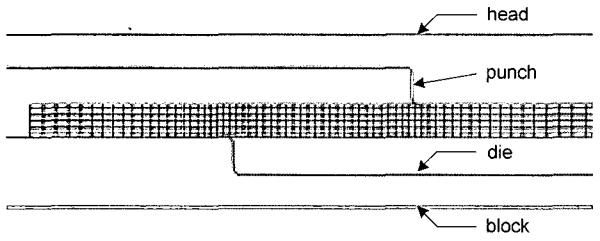

Figure 2. Finite element mesh.

and the block. Since identical half-beads are stacked at the same location, the finite element model for one half-bead is sufficient to assess the stacked half-beads. Since the bead is symmetrical with respect to the centerline of hole, the finite element model is constructed with axisymmetric elements.

Figure 2 shows the finite element mesh of the half-bead. The bead plate consists of 0.2 mm thick SUS 301 plate and 0.025 mm thick NBR (nitril butadiene rubber) coating on both surfaces of the plate. The mesh was constructed with 8-node isoparametric axisymmetric elements. The size of element of SUS plate near the corners of dies was 50 μm×50 μm, and that of NBR coating was 25 μm×25 μm. Although the mesh was relatively coarse, the analysis results differed marginally from those obtained with much finer mesh. Since the residual stresses in the half-bead plate generated during the half-bead forming process have influence on both the sealing performance and the fatigue durability, the forming process was included in the model. The forming punch and die were modeled with rigid bodies. Corner radius of the punch and die were assumed to be 50 μm. The cylinder head and the block were also modeled with rigid bodies.

Figure 3 shows stress-strain curves for the SUS 301 thin plate and the NBR coating. The curve for SUS 301 plate was obtained from uniaxial tensile test with standard thin plate specimen. The curve for NBR coating was obtained from uniaxial tension and compression test with standard dumbbell specimen for test of rubber materials

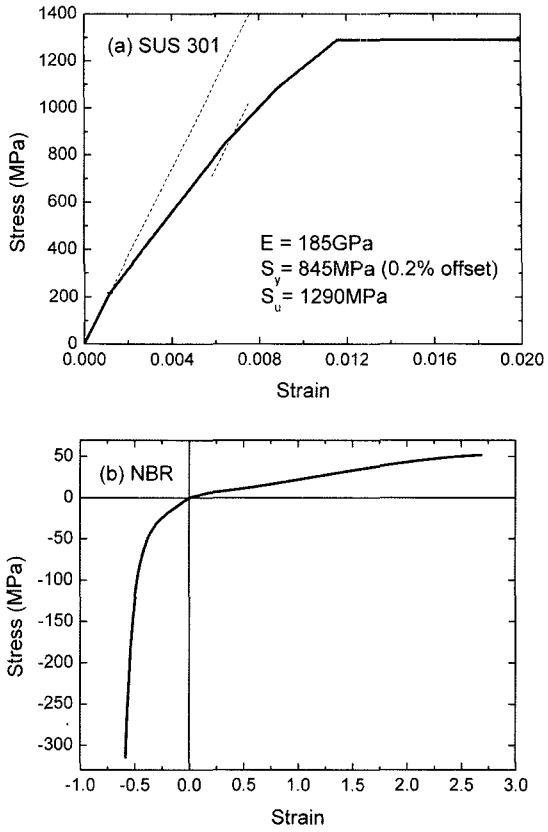

Figure 3. Stress-strain curves for (a) SUS 301 plate and (b) NBR.

that was conducted by the manufacturer of NBR coating material. Based on these curves the SUS 301 plate was assumed as an elasto-plastic material with isotropic hardening, and the NBR as a hyperelastic material. Sliding friction tests of the NBR-coated SUS 301 plate against the steel block gave the friction coefficient in the range from 0.1 to 0.3. Hence, the friction coefficient of the bead plate against all the rigid bodies in the model was set equal to 0.2.

The simulation was conducted with a commercial finite element code ABAQUS. A quasi-static incremental solution technique was employed with nonlinear geometry analysis scheme. No boundary condition was specified for the mesh. That is, the rigid body motion in the radial direction is self-constrained since the model is axisymmetric. The gravitational force was included to prohibit the rigid body motion in the axial direction. The motion of the forming dies was displacement-controlled while that of the head was force-controlled in order to mimic the real situation.

Figure 4 shows the analysis procedure. The analysis starts with the forming simulation of the half-bead. The bead plate is positioned between the punch and the die (Figure 4(a)). The punch is moved down to form the half-

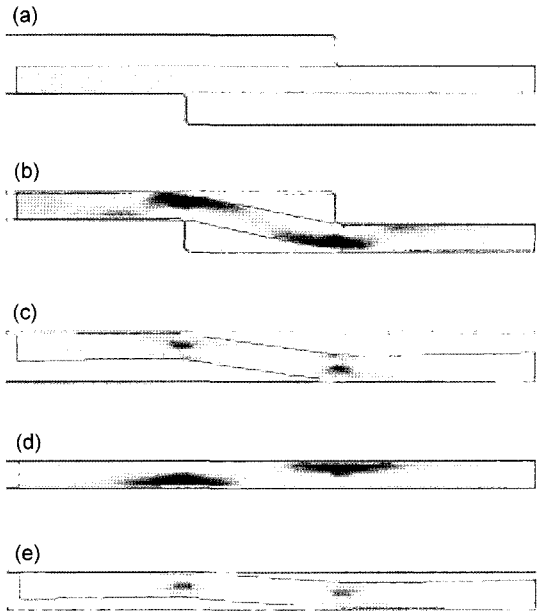

Figure 4. Finite element analysis procedure: (a) beginning of simulation, (b) half-bead forming, (c) positioning of half-bead between head and block, (d) compression of half-bead by head during fastening, and (e) recovery of half-bead due to head lift-off.

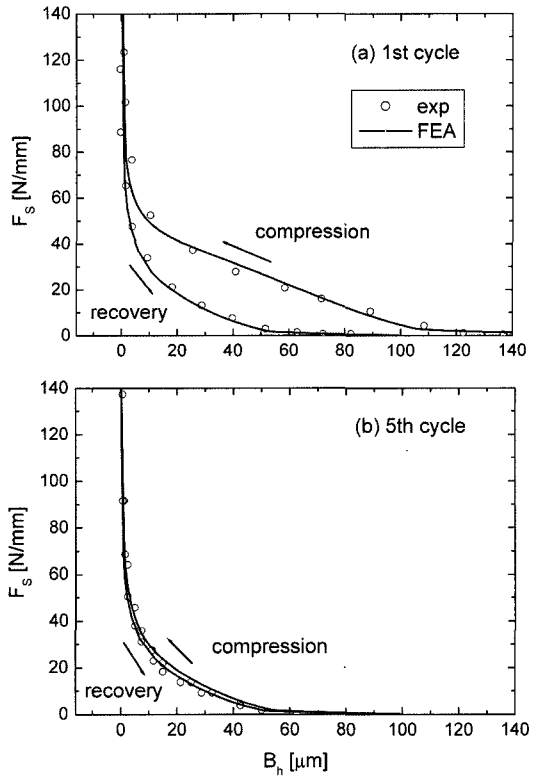

Figure 5. Variation of sealing force with bead height during compression and recovery.

bead (Figure 4(b)), and then moved up to the initial position. After the forming is completed, the punch and the die are removed and the half-bead is positioned between the head and the block (Figure 4(c)). The head is moved down to simulate the installation of half-bead until the fastening load reaches a specified value (Figure 4(d)). And then the head is moved upward to simulate the head lift-off (Figure 4(e)). The up-and-down movement of the head is repeated five times to stabilize the recovery behavior of the half-bead. Data for the assessment of half-bead are obtained during the up-and-down movement of the head with the stabilized half-bead.

3. RESULTS AND DISCUSSION

3.1. Model Verification

Figure 5 shows the variation of sealing force with the half-bead height during the compression and recovery of the half-bead in the first and fifth cycles. The sealing force F_s is the reaction force of the half-bead of unit circumferential length due to the movement of head. The bead height B_h is the instantaneous height of the bead during the compression and the recovery. The compression curve in the first cycle correspond to the fastening of the half-bead, and that in the fifth cycle corresponds to the downward movement of the head with the decrease in the combustion gas pressure. The recovery curve corresponds to the shape recovery of the compressed half-bead during the head lift-off due to the increase in the combustion gas pressure. The curve in the first cycle differs significantly from that in the fifth cycle because of the plastic deformation of the half-bead during the fastening. Figure 5 also shows the experimental data. The analysis result agrees well with the experimental data. Hence, it is claimed that the model simulates the behavior of the half-bead excellently.

3.2. Design Parameter Assessment

Three design parameters, i.e., the unfastened bead height B_{ho}, the bead width B_w, and the radial length of hole-side flat region L_{in} (refer to Figure 1) are assessed with respect to the sealing performance and the fatigue durability. The assessment is conducted by varying the value of each parameters one by one from the case shown in Figure 5 where B_{ho}=0.21 mm, B_w=1.5 mm and L_{in}=1.5 mm. The values of parameters are chosen in the practical range.

Figure 6 shows the variation of sealing force with the head lift-off H_L during the recovery of bead at the fifth cycle for various unfastened bead height B_{ho}. The head lift-off is defined as the height increment of fastened bead resulting from the combustion gas pressure. Since the bead height is almost zero when it is fastened, the head lift-off is almost the same as the bead height shown in

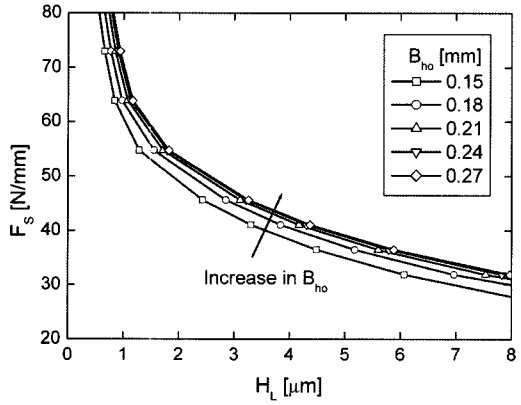

Figure 6. Variation of sealing force with head lift-off for various unfastened bead height.

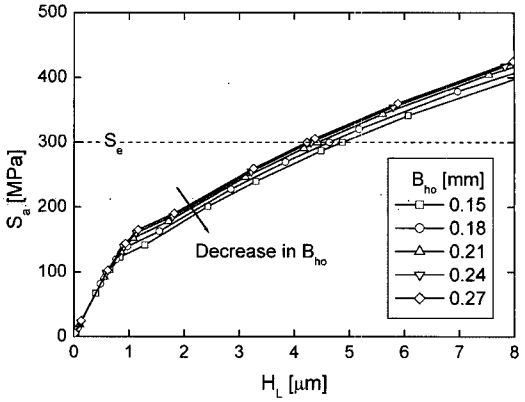

Figure 8. Variation of stress amplitude with head lift-off for various unfastened bead height.

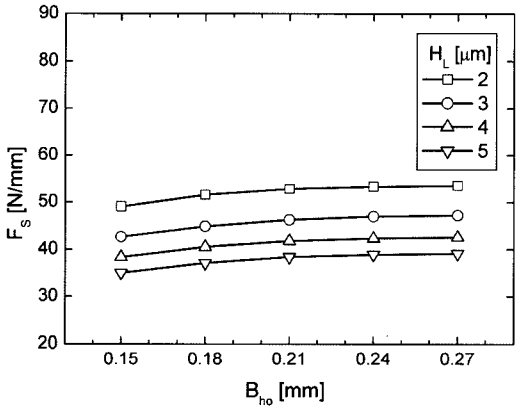

Figure 7. Effect of unfastened bead height on sealing force at various head lift-off.

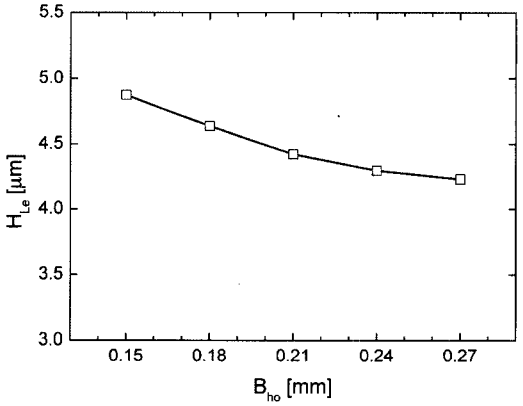

Figure 9. Effect of unfastened bead height on maximum allowable head lift-off.

Figure 5. The curve moves upward slightly with the increase in the unfastened bead height.

The head lift-off is fixed in a given engine structure when the maximum combustion gas pressure is fixed. Since the half-bead must maintain its sealing capability even when the head-block gap is increased due to the head lift-off, the sealing performance can be assessed with the criterion that the half-bead possesses better sealing performance when the sealing force is stronger at a given head lift-off.

Figure 7 shows the variation of sealing force with the unfastened bead height at various head lift-off. This result is obtained from Figure 6. With the increase in the unfastened bead height, the sealing force increases but its increasing rate becomes slower. This result implies that the taller half-bead exhibits better sealing performance but its effect is saturated as the height increases.

The fatigue durability is assessed with the stress amplitude versus fatigue life (S-N) approach in the high cycle fatigue theory because the half-bead is deformed elastically during the compression and recovery. In Figure 4 the darkness in the bead plate represents the level of maximum principal stress. The darker region indicates the greater maximum principal stress. Comparing Figures 4(d) and 4(e), the difference of maximum principal stress is significant at the surface near the bent portions, and the maximum principal stress decreases most rapidly in the thickness direction near the bent portions. Moreover, the direction of maximum principal stress near the bent portions was almost parallel to the surface of the bead plate. According to the high cycle fatigue theory, these results imply that the fatigue crack is generated at the surface near the bent portions of the half-bead, and then propagates through the thickness of the bead plate. This prediction is consistent with the knowledge from experience. Therefore, the amplitude of the maximum principal stress is used to assess the fatigue durability in this study.

Figure 8 shows the variation of maximum stress amplitude S_a in the bead plate with the head lift-off for various unfastened bead height. The stress amplitude increases with the head lift-off, and cross the endurance

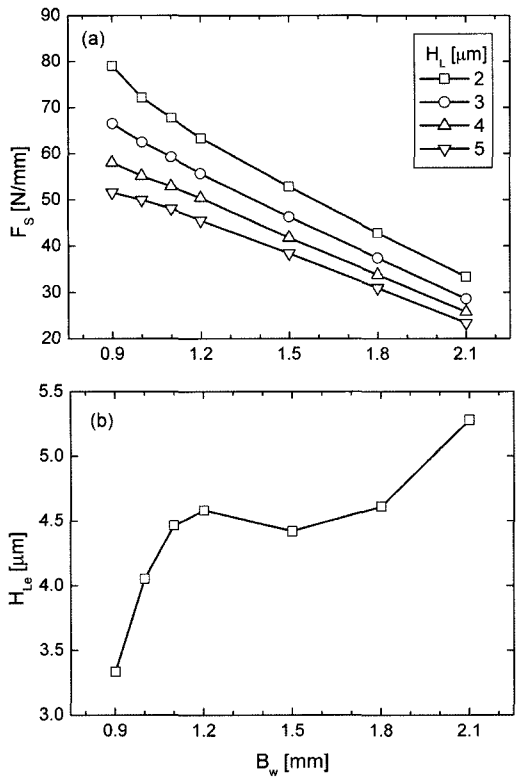

Figure 10. Effects of bead width on (a) sealing force at various head lift-off and (b) maximum allowable head lift-off.

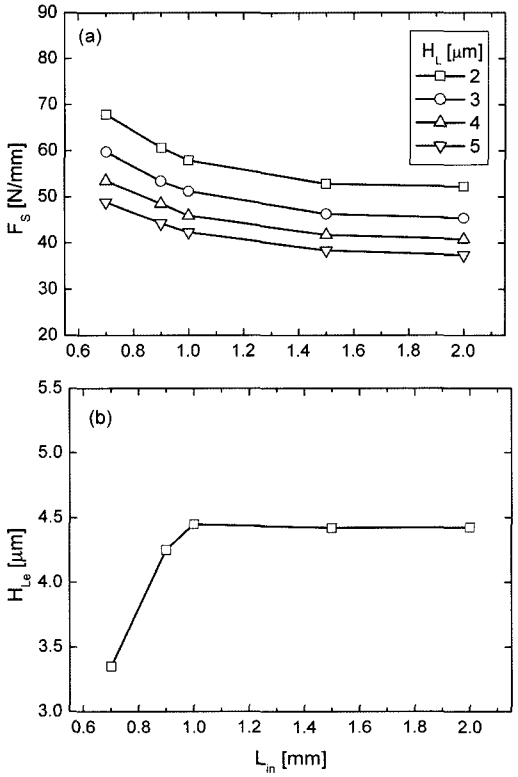

Figure 11. Effect of radial length of hole-side flat region on (a) sealing force at various head lift-off and (b) maximum allowable head lift-off.

limit of the bead plate S_e=300 MPa (Han *et al.*, 2004; Cho *et al.*, 2005). The effect of mean stress on the endurance limit is disregarded because the uniaxial fatigue tests with standard thin plate specimen revealed marginal influence of mean stress on the endurance limit in the practical stress range of beads (Han *et al.*, 2004). Since the fatigue failure does not occur when the stress amplitude is lower than the endurance limit, the head lift-off at which the stress amplitude reaches the endurance limit is the maximum allowable head lift-off H_{Le} for prevention of fatigue failure. Since the gasket is designed to assure the infinite fatigue life, the maximum allowable head lift-off is used for assessment in this study. The assessment criterion is that the half-bead possessing the greater maximum allowable head lift-off exhibits better fatigue durability.

Figure 9 shows the variation of maximum allowable head lift-off with the unfastened bead height. This result is obtained from Figure 8. The maximum allowable head lift-off decreases with the increase in the unfastened bead height. This means that the taller half-bead is more susceptible to the fatigue failure. The results about the effect of unfastened half-bead height can be summarized that the increase in the unfastened bead height improves the sealing performace but deteriorates the fatigue durability.

Figure 10 shows the effects of half-bead width B_w on the sealing force and the maximum allowable head lift-off. According to Figure 10(a), the sealing force is reduced as the half-bead width increases. According to Figure 10(b), the maximum allowable head lift-off increases rapidly with the bead width when the bead width is smaller than 1.2 mm or greater than 1.8 mm. When the bead width is between 1.2 mm and 1.8 mm, the maximum allowable head lift-off exhibits marginal dependence on the bead width although the value at B_w=1.5 mm is slightly lower. It can be summarized that as the bead width is decreased in a range between 1.2 mm and 1.8 mm, the sealing performance is enhanced without significant change in the fatigue durability. Outside of the range, improvement of the sealing performance is accompanied by the loss of fatigue durability. It is noted that the bead width has stronger influence than the unfastened bead height.

Figure 11 shows the effects of radial length of hole-side flat region L_{in} on the sealing force and the maximum allowable head lift-off. According to Figure 11(a), the sealing force decreases as the flat region becomes longer.

However, when the length is longer than 1.5 mm, its effect is marginal. According to Figure 11(b), when the flat region length is shorter than 1 mm, the maximum allowable head lift-off decreases with the loss of the flat region length. When it is longer than 1 mm, it has marginal influence. These results indicate that the flat region length has marginal influence when it is greater than 1.5 mm. As the length is reduced from 1.5 mm to 1 mm, the sealing performace improves without the deterioration of fatigue durability. Further loss of the length enhances the sealing performance at the sacrifice of the fatigue durability.

4. CONCLUSION

A finite element model of half-bead has been developed to assess the sealing performance and the fatigue durability. The reliability of the model was verified with the experimental data. The model was employed to examine the design parameters of half-bead, and the following results were obtained.

In a certain range of the bead width (from 1.2 mm and 1.8 mm in the present study), the loss of the width improves the sealing performance without significant change in the fatigue durability. Outside of the range, the improvement of sealing performance is accompanied by the deterioration of fatigue durability as the width is reduced. The bead width has stronger influence than the other parameters.

The increase in the unfastened bead height improves the sealing performace but deteriorates the fatigue durability. However, this parameter has relatively marginal influence.

The flat region length has marginal influence when it is relatively long. As the length is reduced, the sealing performace is enhanced gradually, whereas the fatigue durability is decreased rapidly when the length is shorter than a certain value (1 mm in the present study).

REFERENCES

Cho, S.-S., Han, B. K., Chang, H. and Kim, B. K. (2005). Effects of forming process on sealing performance of full-bead of MLS gasket: finite element analysis approach. *Int. J. Automotive Technology* **6**, **2**, 191–196.

Cho, S.-S., Han, B. K., Lee, J. H., Chang, H. and Kim, B. K. (2005). Fatigue durability assessment of full-bead of MLS gasket using finite element analysis. *Int. J. Automotive Technology* **6**, **5**, 513–517.

Han, B. K., Cho, S.-S., Chang, H. and Kim, B. K. (2004). Fatigue fracture of NBR-coated SUS301 thin plate for MLS gasket. *Trans. Korea Society of Automotive Engineers* **12**, **4**, 207–212.

Harland, C., Novaria, P. and Robinson, M. (1993). Process and Performance Modeling of Gasket Components. *SAE Paper No.* 930118.

Ishigaki, T., Kitagawa, J. and Tanaka, A. (1993). New evaluation method of metal head gasket. *SAE Paper No.* 930122.

Popielas, F., Chen, C. and Obermaier, S. (2000). CAE approach for multi-layer steel cylinder head gaskets. *SAE Paper No.* 2000-01-1348.